Stationarity of the tropical pacific teleconnection to North America in CMIP5/PMIP3 model simulations

Sloan Coats,[1] Jason E. Smerdon,[1] Benjamin I. Cook,[2] and Richard Seager[1]

Received 26 June 2013; revised 28 August 2013; accepted 6 September 2013.

[1] The temporal stationarity of the teleconnection between the tropical Pacific Ocean and North America (NA) is analyzed in atmosphere-only, and coupled last-millennium, historical, and control runs from the Coupled Model Intercomparison Project Phase 5 data archive. The teleconnection, defined as the correlation between December-January-February (DJF) tropical Pacific sea surface temperatures (SSTs) and DJF 200 mb geopotential height, is found to be nonstationary on multidecadal timescales. There are significant changes in the spatial features of the teleconnection over NA in continuous 56-year segments of the last millennium and control simulations. Analysis of atmosphere-only simulations forced with observed SSTs indicates that atmospheric noise cannot account for the temporal variability of the teleconnection, which instead is likely explained by the strength of, and multidecadal changes in, tropical Pacific Ocean variability. These results have implications for teleconnection-based analyses of model fidelity in simulating precipitation, as well as any reconstruction and forecasting efforts that assume stationarity of the observed teleconnection.
Citation: Coats, S., J. E. Smerdon, B. I. Cook, and R. Seager (2013), Stationarity of the tropical pacific teleconnection to North America in CMIP5/PMIP3 model simulations, *Geophys. Res. Lett.*, *40*, doi:10.1002/grl.50938.

1. Introduction

[2] The tropical Pacific Ocean impacts regional hydroclimate variability in the extratropics by means of wave propagation from areas of persistent precipitation and divergence anomalies that are in turn forced by sea surface temperature (SST) variations [e.g., *Sarachik and Cane*, 2010]. The preferred circulation responses to tropical Pacific SST forcing are called atmospheric teleconnections and depend on a Rossby wave response (see *Trenberth et al*. [1998], for a review) and subsequent interaction between the mean flow anomaly and transient eddies [*Hoerling and Ting*, 1994; *Seager et al*., 2003, 2010; *Harnik et al*., 2010]. A quintessential feature of the El Niño-Southern Oscillation (ENSO) teleconnection is the Pacific jet stream shift over the western coast of North America (NA), which a wealth of research has implicated as an important forcing of hydroclimate variability in NA on interannual to decadal timescales [e.g., *Dettinger et al*., 1998; *Schubert et al*., 2004a, 2004b; *Seager et al*., 2005a, 2005b, 2008; *Herweijer et al*., 2006].

[3] The basis of our understanding of atmospheric teleconnections, between ENSO and NA or otherwise, is derived from the temporally limited observational record and associated reanalysis products [*Trenberth et al*., 1998]. The stationarity of teleconnections is important for understanding the impact of internal variability and forced responses within the climate system, an understanding that is fundamental to robust projections of regional climate change in a warming world. Within the approximately 100-year observational record, there is evidence that teleconnection patterns can vary considerably in space and time [e.g., *Hu and Feng*, 2001; *Rajagopalan et al*., 2000; *Cole and Cook*, 1998; *Gershunov and Barnett*, 1998]. A characterization of the stationarity of teleconnection patterns on decadal-to-centennial timescales, however, is not possible using only reanalysis and observational data because of their limited temporal extent. These limitations necessitate the use of alternative approaches to further characterize and understand teleconnection stationarity spanning decades and centuries. Toward such ends, multiple model products from the recent and ongoing release of the fifth Coupled Model Intercomparison Project (CMIP5) [*Taylor et al*., 2012] and third Paleoclimate Model Intercomparison Project (PMIP3) provide a state-of-the-art ensemble of model simulations for evaluating and testing teleconnection stationarity over multiple timescales.

[4] Here we analyze three ensembles of fully-coupled Atmosphere-ocean General Circulation Models from the CMIP5/PMIP3 archive and compare them to the National Centers for Environmental Prediction/National Center for Atmospheric Research (NCEP/NCAR) reanalysis project 1 [*Kalnay et al*., 1996] to assess the stationarity of the modeled ENSO-NA teleconnection. Our analyses suggest considerable variability in the simulated character of the teleconnection across the model ensemble on multidecadal timescales. These findings are crucial for assessments of model fidelity that often use regional teleconnection strength and spatial features as an evaluation metric, particularly with regard to simulated precipitation variability [e.g., *Jospeh and Nigam*, 2006; *Smith and Chandler*, 2010; *Weare*, 2012; *Langenbrunner and Neelin*, 2013; *Polade et al*., 2013]. Furthermore, if realistic, these findings have important implications for forecasting [e.g., *Barnston et al*., 2010] and reconstruction [e.g., *MacDonald and Case*, 2005; *D'Arrigo et al*., 2005] efforts that rely on the stationarity of teleconnection characteristics as defined by the observational interval.

Additional supporting information may be found in the online version of this article.

[1]Lamont Doherty Earth Observatory, Palisades, New York, USA.
[2]NASA Goddard Institute of Space Studies, New York, New York, USA.

Corresponding author: S. Coats, Lamont Doherty Earth Observatory, 103B Oceanography, 61 Route 9W - PO Box 1000, Palisades, NY 10964-8000, USA. (sjc2164@columbia.edu)

0094-8276/13/10.1002/grl.50938

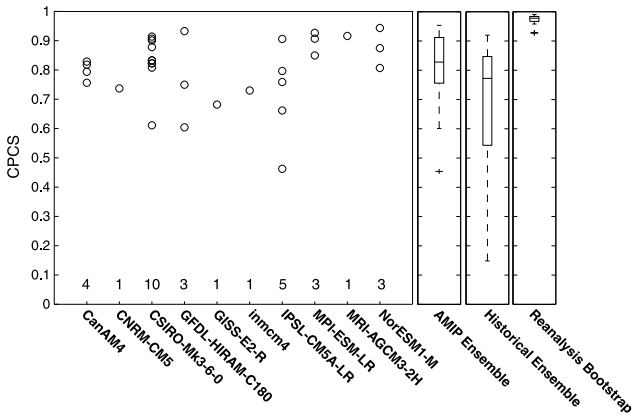

Figure 1. Teleconnection stationarity, as measured by the CPCS over NA, using teleconnection patterns estimated from the NCEP-NCAR reanalysis (see Figure 2) and the AMIP simulations. The first panel on the left is the CPCS value for each AMIP simulation. The second panel from the left plots the CPCS range for all 32 AMIP simulations. The third panel is the CPCS range for the 1979–2005 C.E. period in the 16 coupled historical runs. The last panel on the right is the CPCS range for the reanalysis bootstrap experiment. Box plots represent the 25th and 75th percentiles of the data with the mean as the central line and the whiskers showing the full data range excluding outliers; outliers are marked with a cross (larger than 75th +1.5(75th −25th) or smaller than 25th −1.5(75th −25th)). The number of ensemble members from each AMIP model are the values inset in the main panel.

2. Data

[5] All model output is from the CMIP5/PMIP3 archive. The three fully-coupled model ensembles are (1) 16 historical runs (1850–2005 Common Era (C.E.)) that have been forced with a common set of time-varying estimates of incident solar radiation, volcanic activity, and atmospheric constituents; (2) sixteen 500-year control simulations with constant preindustrial (pre-1850 C.E.) boundary conditions using the same models as in the collection of historical runs [*Taylor et al*., 2012]; and (3) seven last-millennium (LM) simulations (850–1850 C.E.) forced with reconstructed time-varying exogenous forcing conditions [*Schmidt et al*., 2011]. As a compliment to the fully-coupled runs, we use an uncoupled atmosphere-only ensemble comprising 10 sets of atmosphere model simulations with ensemble sizes between 1 and 10 from the Atmospheric Model Intercomparison Project (AMIP—a total of 32 simulations). Each ensemble member consists of an atmospheric simulation forced with the same observed SST boundary conditions for the period 1979–2008 C.E. All output from the above collection of simulations has been regridded to a common 2.5° × 2.5° latitude-longitude grid to match the reanalysis data set (for 66% of the simulations this represents a spatial degradation of the data).

[6] The reanalysis data are taken from the National Oceanic and Atmospheric Administration NCEP/NCAR Climate Data Assimilations System 1 project [*Kalnay et al*., 1996]. The monthly-resolved data span the period 1949–2012 C.E. on an equal area 2.5° × 2.5° latitude-longitude grid. The reanalysis product uses a frozen analysis/forecast system with data assimilation of past observations and is an established data set for assessment of interannual upper-air variability.

3. Twentieth Century Teleconnection Variability

[7] The analyzed model fields are surface temperature and 200 mb geopotential height. The latter was chosen over precipitation because it comprises a more spatially and temporally homogeneous representation of the NA teleconnection, and because it is the ultimate driver of the precipitation variability. For both fields, the climatology (calculated over the full simulations and the full length of the reanalysis) has been removed and the December-January-February (DJF) anomalies averaged. Winter averages were chosen because winter is the dominant period of precipitation forcing by ENSO in Western NA [*Trenberth et al*., 1998].

[8] The teleconnection is defined by the grid point correlation between the DJF average 200 mb geopotential height fields and the DJF average Niño 3.4 (170°W–120°W, 5°N–5°S) SST index. The resulting correlation field indicates both the teleconnection strength and its spatial features. As an estimate of the observed teleconnection pattern, the correlation field was calculated for two periods in the NCEP-NCAR reanalysis: 1949–2005 C.E. (the overlapping period with the historical runs) and 1979–2005 C.E. (the overlapping period with the AMIP runs). To assess the modeled teleconnection over NA, the centered pattern correlation statistic (hereinafter CPCS—following *Santer et al*. [1995]) was calculated between these reanalysis teleconnection patterns and the teleconnection patterns from the models over the NA region (160°W–50°W, 70°N–20°N). The CPCS is equivalent to a Pearson's product-moment linear correlation between spatial values [*Santer et al*., 1995].

[9] Figure 1 characterizes the teleconnection variability across the collection of AMIP models and within the individual model ensembles. For each AMIP ensemble member, a teleconnection pattern was calculated and compared to the 27-year period from the reanalysis using the CPCS. Because each simulation is forced with the same observed SSTs, the range in CPCS within each AMIP model ensemble represents an estimate of the impact of internal atmospheric variability on the circulation over NA. The calculated range was subsequently compared to the pattern correlation range from the same period in the historical runs, which have coupled SSTs, and thus different SST variability and patterns. When all of the AMIP simulations are considered (32 in total), the CPCS range (excluding outliers) is about 0.35 (Figure 1). This is less than half the range over the same period (1979–2005 C.E.) in the coupled historical runs with dynamically evolving SSTs (Figure 1). Atmospheric noise, therefore, cannot be considered the dominant driver of differences between modeled teleconnections over NA in the collection of model simulations, and the relative differences in the range of the CPCS statistic are interpreted as arising from the SST-induced variations on the teleconnection over NA in the coupled simulations. For a further discussion of this analysis and interpretation, see the supporting information.

[10] To evaluate the temporal stationarity of the observed teleconnection in the reanalysis data over a 27-year window, a bootstrap resampling of CPCS values in continuous 27-year segments was computed over the 56-year reanalysis record. The range in CPCS for 1000 of these resampled segments against the 1979–2005 C. E. reanalysis target is also plotted in Figure 1. The narrow range indicates that the character of the reanalysis teleconnection in the 27-year overlapping period between the AMIP and historical simulations is well represented relative to the full 56-year period of the reanalysis.

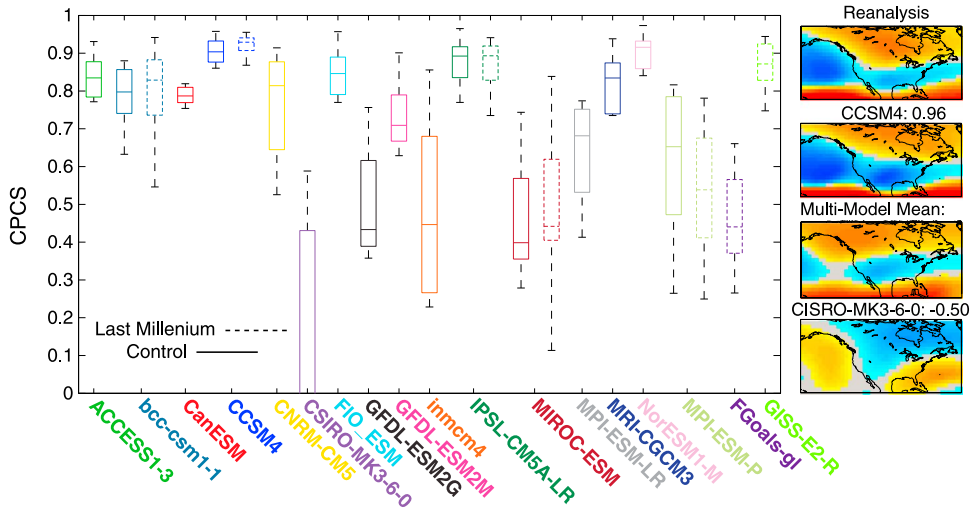

Figure 2. Teleconnection stationarity, as measured by the CPCS over NA, using teleconnection patterns estimated from the NCEP-NCAR reanalysis and nonoverlapping 56-year segments from the 500-year control (solid boxes) and 1000-year forced LM runs (dashed boxes). Box plots indicate the 75th and 25th percentile of the CPCS statistic across the segments in the respective coupled model runs with the mean as the central line and the whiskers showing the full data range excluding outliers (larger than 75th +1.5(75th −25th) or smaller than 25th −1.5(75th −25th)). The right four panels are the teleconnection pattern over 160°W–50°W, 70°N–20°N for the (first panel) reanalysis, (second and fourth panels) the most and least realistic segments, respectively, and the (third panel) model ensemble average. The colorbar range is −1-blue to 1-red. LM ranges have been included as per their availability in the PMIP3 archive. Only models with 500-year control simulations were included, as a consequence, the GISS-E2-R and F-Goals models only have a LM simulation.

4. Multidecadal Teleconnection Variability

[11] To investigate the nature of teleconnection stationarity over longer timescales, the control and LM runs were divided into 56-year segments to match the length of the NCEP/NCAR reanalysis record, generating a time-slice ensemble of 17 members for each LM run and eight members for each control run. For each segment, the correlation between the Niño 3.4 index and the 200 mb geopotential height field was calculated and compared to the 56-year (1949–2005 C.E.) pattern from the reanalysis, again using the CPCS. The range in the CPCS is thus interpreted as a measure of the temporal stationarity of the teleconnection within a given model.

[12] The range of CPCS for the 16 control and seven LM runs is shown in Figure 2 and indicates a wide range in the teleconnection character within and between models. The models that have a stationary teleconnection (small range in CPCS values) in the control runs possess a similarly stationary teleconnection in the corresponding LM runs (e.g., Community Climate System Model version 4 (CCSM4)). The converse is also true (e.g., Model for Interdisciplinary Research on Climate Earth System Model (MIROC-ESM) and Max Planck Institute for Meteorology Earth System Model (MPI-ESM-P)). Transient forcing characteristics therefore do not appear to significantly impact the simulated teleconnection stationarity.

[13] There is considerable spread in the CPCS range between models. For instance, the CCSM4 model simulates a stationary teleconnection that is consistently comparable to the reanalysis data. Canadian Earth System Model (CanESM) is likewise stationary but less consistent with the reanalysis pattern, while the teleconnection simulated by the Commonwealth Scientific and Industrial Research Organization (CSIRO)-Mk3-6-0 model is neither stationary nor consistent with the reanalysis pattern. These observations are not explained by model resolution: while the CCSM4 model has the highest resolution of the simulations (0.9° × 1.3°), CanESM is relatively low resolution (2.8° × 2.8°) and CSIRO-Mk3-6-0 is in between (1.9° × 1.9°). We therefore investigate below the potential dynamical links between variability in tropical Pacific SSTs and changing teleconnection characteristics over NA.

5. Potential Dynamical Influences on Temporal Teleconnection Variability

[14] What might cause the teleconnection over NA to be nonstationary? The dynamics of teleconnection variability within the models are not fully explored herein, but our analysis suggests that a significant role is played by both the strength and spatial features of the SST anomalies in the tropical Pacific.

[15] We use the Center of Heat Index (CHI) [*Giese and Ray*, 2011] as a measure of the strength and location of SST anomalies in the tropical Pacific. The CHI statistic is analogous to the first moment of the SST anomaly field and provides both an amplitude and mean longitude for each ENSO event. Figures 3a and 3b plot average CHI amplitudes for each 56-year segment from the 16 control runs against the CPCS over NA during the same segment to assess the impact of the magnitude of ENSO events on the teleconnection. Segments with larger El Niño and La Niña events have higher values of the CPCS, although the connection is weak (Figures 3a and 3b). The same analysis was completed for CHI longitude and a much weaker relationship between eastward CHI longitude anomalies and high values of CPCS over NA was found (not shown).

[16] Figure 3c investigates the impact of a model's tropical Pacific SST variability on teleconnection stationarity by plotting the average variance of the Niño3.4 index for each time-slice ensemble against the range in the CPCS. There is a significant positive relationship between the ENSO amplitude

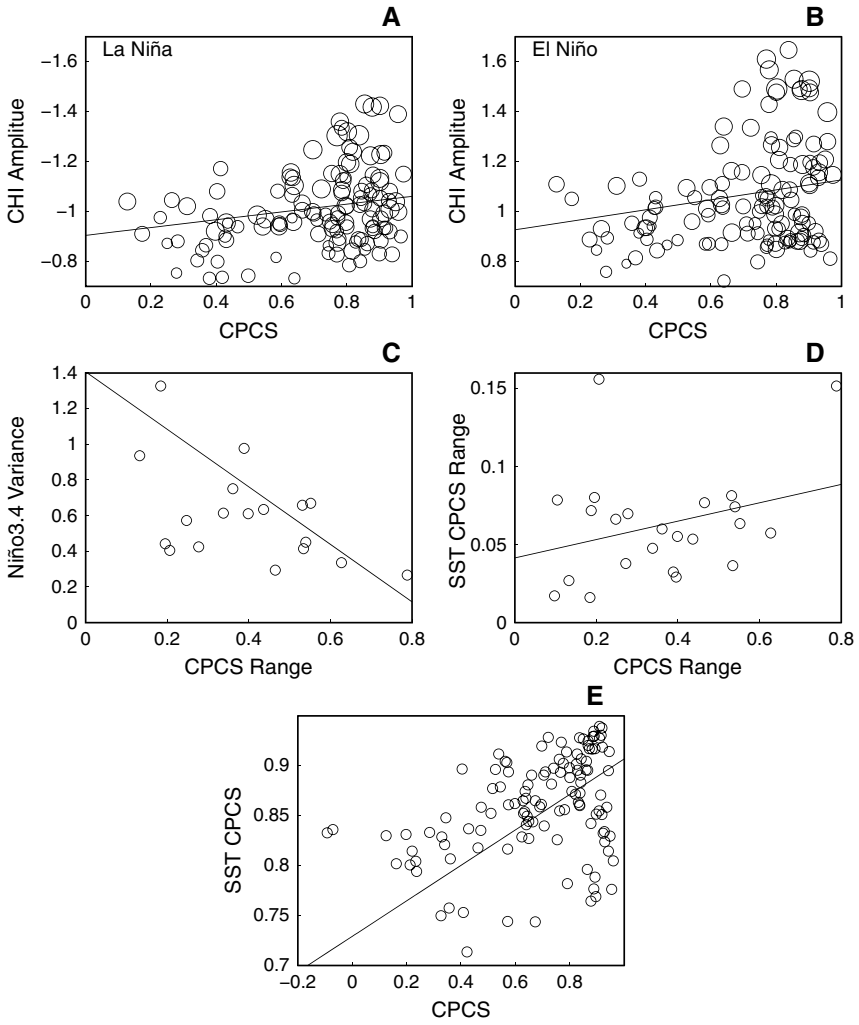

Figure 3. Average CHI amplitude for (a) La Niñas and (b) El Niños in each 56-year segment plotted against the CPCS for that segment in the model control runs. The circle radius is proportional to the number of ENSO events in each segment. (c) The variance of the Niño3.4 index for the full control and LM simulations against the range in CPCS for that model simulation. (d) The range in the CPCS of the first EOF of tropical Pacific SSTs for the time-slice ensemble against the teleconnection CPCS range. (e) The CPCS of the first EOF of tropical Pacific SSTs from the top eight segments of each control run (see methods for ranking criteria) with that from the NCEP-NCAR reanalysis plotted against the CPCS of the NA teleconnection for that segment. The lines on each panel are the linear regression lines calculated using ordinary least squares. (See Table 1 for regression statistics.)

and teleconnection stationarity, suggesting that large tropical Pacific SST variability allows the associated teleconnection to emerge above noise from secondary patterns of variability. For a discussion of this result in relation to the role of internal atmospheric variability in teleconnection stationarity, see the supporting information.

[17] To determine the impact of the stationarity of the modeled ENSO spatial patterns on teleconnection stationarity, we compute the first empirical orthogonal function (EOF) of the DJF tropical Pacific SST anomaly (defined as 120°E–60°W, 30°N–30°S) for each segment of the control and LM simulations and compare them, using the CPCS statistic, to the same field from the reanalysis. This EOF was determined to be representative of ENSO by a strong correlation (average Pearson's correlation coefficient of 0.96 for all control and LM segments) between its principal component time series and the Niño3.4 index. In Figure 3d, the range in the CPCS between the model and reanalysis EOFs is compared to teleconnection stationarity to determine if models with large multidecadal variability in the spatial expression of ENSO have nonstationary teleconnections. There is a weak positive relationship, indicating that temporal changes in the spatial character of ENSO exert a limited control on the stationarity of the NA teleconnection.

[18] To further characterize the spatial nature of modeled ENSO, the first EOF of the DJF tropical Pacific SST anomaly was calculated for each control run using a 56-year sliding

Table 1. Pearson's Coefficient of Determination (R^2), *P* Values (*P* val), and Mean Squared Error (MSE) for the Linear Least Squares Regression Derived From the Variable Associations Shown in Figures 3a–3e

Figure 3	R^2	*P* Val	MSE
(a)	0.068	0.003	0.022
(b)	0.063	0.004	0.040
(c)	0.336	0.003	0.175
(d)	0.096	0.157	0.000
(e)	0.399	0.000	0.000

window (incremented by 1 year, thus including overlap) and compared, using the CPCS statistic, to the same field from the reanalysis. The top eight segments for each simulation, as determined by the largest variance explained by the first mode of tropical ocean variability, were subsequently chosen for analysis. This method of segment identification was done in order to maximize the ENSO-forced extratropical atmospheric signal, using the rationale that segments with a dominant first mode of tropical Pacific Ocean variability will contain less "noise" from secondary patterns in the tropical Pacific Ocean. Additionally, there is a 0.86 correlation between the variance of the Niño3.4 index and the percent variance explained by the first EOF across all models, thus the identified segments will also have the largest ENSO amplitude. The results are plotted in Figure 3e and indicate that the modeled and observed teleconnection will compare well when both strong ENSO variability exists and when the model's ENSO spatial features match those of the reanalysis.

[19] The statistical significance of the relationships in Figure 3 is investigated using Pearson's correlation coefficients. Despite our use of this metric for a quantitative description of the variable associations, there is no reason to assume that the functional form is linear or that the relationship can be fully captured given the small sample size. While there is clearly a relationship between temporal and spatial changes in ENSO and the NA teleconnection, the correlations are weak (Table 1). This is not surprising given other sources of atmosphere-ocean variability. Nevertheless, the correlation in Figure 3e, our best attempt to isolate the signal of the ENSO spatial pattern and amplitude, indicates a moderate and statistically significant relationship.

6. Discussion and Conclusion

[20] The similarity of the ENSO-NA teleconnection between coupled model simulations and the observational record over the historical interval is an often used metric of model fidelity in reproducing coupled ocean-atmosphere dynamics [e.g., *Joseph and Nigam*, 2006; *Smith and Chandler*, 2010; *Polade et al*., 2013]. We nevertheless have shown that many models exhibit considerable variability in their teleconnection strength and character during different 56-year windows of continuous simulations. These results suggest that analyses of teleconnection fidelity should be limited to atmosphere-only simulations forced with observed SSTs [e.g., *Langenbrunner and Neelin*, 2013]. Furthermore, considerable variability in modeled ENSO on multidecadal-to-centennial timescales has been reported in the literature [e.g., *Wittenberg*, 2009; *Karnauskas et al*., 2012; *Ogata et al.,* 2013]. If such modeled behavior is dynamically realistic and drives changes in the atmospheric teleconnections, the 56-year reanalysis period may not be sufficient for adequately representing the character of the teleconnection over long timescales. In particular, the impact of nonstationary teleconnections on regional precipitation variability must be better understood, particularly given the range of reconstruction [e.g., *MacDonald and Case* 2005 and *D'Arrigo et al*., 2005] and forecasting efforts (see *Barnston et al*. [2010] for a review of seasonal forecasting efforts) that rely on the stationarity of the observed teleconnection.

[21] Our conclusions also have important implications for efforts to explain the hydroclimate history of western North America and its links to tropical Pacific climate variations. In particular, further characterizations of inter-model differences and outliers, as well as a more robust analysis of the coupled atmosphere ocean dynamics that drive temporal variations in simulated teleconnections, will provide improved understanding of teleconnection behavior and model performance. Furthermore, attempts must be made to relate teleconnection fidelity and stationarity to hydroclimate impacts on decadal to multidecadal timescales [e.g., *Coats et al*., 2013; also in preparation, 2013]. Such efforts will improve characterizations of uncertainties in future projections of regional hydroclimate tied to large-scale teleconnections.

[22] **Acknowledgments.** This work was supported by NOAA award NA10OAR4310137 (Global Decadal Hydroclimate Variability and Change, GloDecH) and NSF award ATM09-02716. We acknowledge the World Climate Research Programme's Working Group on Coupled Modelling, which is responsible for CMIP, and we thank the climate modeling groups (listed in Table S1) for producing and making available their model output. For CMIP, the U.S. Department of Energy's Program for Climate Model Diagnosis and Intercomparison provides coordinating support and led development of software infrastructure in partnership with the Global Organization for Earth System Science Portals LDEO contribution 7723.

[23] The Editor thanks two anonymous reviewers for assistance in evaluating this paper.

References

Barnston, A. G., S. Li, S. J. Mason, D. G. DeWitt, L. Goddard, and X. Gong (2010), Verification of the first eleven years of IRI's seasonal climate forecasts, *J. Appl. Meteorol. Climatol.*, *49*, 493–520.

Coats, S., J. E. Smerdon, R. Seager, B. I. Cook, and J. F. González-Rouco (2013), Megadroughts in southwest North America in millennium-length ECHO-G simulations and their comparison to proxy drought reconstructions, *J. Clim.*, doi:10.1175/JCLI-D-12-00603.1.

Cole, J. E., and E. R. Cook (1998), The changing relationship between ENSO variability and balance in the continental United States, *Geophys. Res. Lett.*, *25*, 4529–4532.

D'Arrigo, R. D., E. R. Cook, R. J. Wilson, R. Allan, and M. E. Mann (2005), On the variability of ENSO over the past six centuries, *Geophys. Res. Lett.*, *32*, L03711, doi:10.1029/2004GL022055.

Dettinger, M. D., D. R. Cayan, H. F. Diaz, and D. M. Meko (1998), North-south precipitation patterns in western North America on interannual-to-decadal timescales, *J. Clim.*, *11*, 3095–3111.

Gershunov, A., and T. P. Barnett (1998), ENSO influence on intraseasonal extreme rainfall and temperature frequencies in the contiguous United States: Observations and model results, *J. Clim.*, *11*(7), 1575–1586.

Giese, B. S., and S. Ray (2011), El Niño in simple ocean data assimilation (SODA), 1781–2008, *J. Geophys. Res.*, *116*, C02024, doi:10.1029/2010JC006695.

Harnik, N., R. Seager, N. Naik, M. Cane, and M. Ting (2010), The role of linear wave refraction in the transient eddy-mean flow response to tropical Pacific SST anomalies, *Q. J. R. Meteorol. Soc.*, *136*, 2132–2146.

Herweijer, C., R. Seager, and E. R. Cook (2006), North American droughts of the mid to late nineteenth century: A history, simulation and implication for Mediaeval drought, *Holocene*, *16*(2), 159–171.

Hoerling, M. P., and M. Ting (1994), Organization of extratropical transients during El Niño, *J. Clim.*, *7*, 745–766.

Hu, Q., and S. Feng (2001), Variations of teleconnection of ENSO and interannual variation in summer rainfall in the central United States, *J. Clim.*, *14*(11), 2469–2480.

Joseph, R., and S. Nigam (2006), ENSO evolution and teleconnections in IPCC's twentieth century climate simulations: Realistic representation?, *J. Clim.*, *19*, 4360–4376.

Kalnay, E., et al. (1996), The NCEP/NCAR 40-year reanalysis project, *Bull. Am. Meteorol. Soc.*, *77*(3), 437–471.

Karnauskas, B. K., J. E. Smerdon, R. Seager, and J. F. Gonzalez-Rouco (2012), A Pacific centennial oscillation predicted by coupled GCMs, *J. Clim.*, *25*, 5943–5961.

Langenbrunner, B., and J. D. Neelin (2013), Analyzing ENSO teleconnections in CMIP models as a measure of model fidelity in simulating precipitation, *J. Clim.*, *26*, 4431–4446, doi:10.1175/JCLI-D-12-00542.1.

MacDonald, G. M., and R. A. Case (2005), Variations in the pacific oscillation over the past millennium, *Geophys. Res. Lett.*, *32*, L08703, doi:10.1029/2005GL022478.

Ogata, T., X. Shang-Ping, A. Wittenberg, and D. Sun (2013), Interdecadal amplitude modulation of El Niño-Southern Oscillation and its impact on tropical Pacific decadal variability, *J. Clim.*, *26*, 7280–7297.

Polade, S. D., A. Gershunovm, D. R. Cayan, M. D. Dettinger, and D. W. Pierce (2013), Natural climate variability and teleconnections to precipitation over the Pacific-North American region in CMIP3 and CMIP5 models, *Geophys. Res. Lett.*, *40*, 2296–2301, doi:10.1002/grl.50491.

Rajagopalan, B., E. R. Cook, U. Lall, and B. K. Ray (2000), Spatiotemporal variability of ENSO and SST teleconnections to summer drought over the United States during the twentieth century, *J. Clim.*, *13*(24), 4244–4255.

Santer, B. D., K. E. Taylor, T. M. L. Wigley, J. E. Penner, P. D. Jones, and U. Cubasch (1995), Towards the detection and attribution of an anthropogenic effect on climate, *Clim. Dyn.*, *12*, 77–100.

Sarachik, E. S., and M. A. Cane (2010), *The El Niño-Southern Oscillation Phenomenon*, Cambridge University Press, Cambridge, United Kingdom.

Schmidt, G. A., et al. (2011), Climate forcing reconstructions for use in PMIP simulations of the last millennium (v1.0), *Geosci. Model Dev.*, *4*, 33–45, doi:10.5194/gmd-4-33-2011.

Schubert, S. D., M. J. Suarez, P. J. Pegion, R. D. Koster, and J. Bacmeister (2004a), Causes of long-term drought in the US Great Plains, *J. Clim.*, *17*(3), 485–503.

Schubert, S. D., M. J. Suarez, P. J. Pegion, R. D. Koster, and J. Bacmeister (2004b), On the cause of the 1930s Dust Bowl, *Science*, *303*(5665), 1855–1859.

Seager, R., N. Harnik, Y. Kushnir, W. Robinson, and J. Miller (2003), Mechanisms of hemispherically symmetric climate variability, *J. Clim.*, *16*(18), 2960–2978.

Seager, R., N. Harnik, W. A. Robinson, Y. Kushnir, M. Ting, H. P. Huang, and J. Velez (2005a), Mechanisms of ENSO-forcing of hemispherically symmetric precipitation variability, *Q. J. R. Meteorol. Soc.*, *131*, 1501–1527.

Seager, R., Y. Kushnir, C. Herweijer, N. Naik, and J. Velez (2005b), Modeling of tropical forcing of persistent droughts and pluvials over western North America: 1856–2000, *J. Clim.*, *18*, 4065–4088.

Seager, R., R. Burgman, Y. Kushnir, A. Clement, E. Cook, N. Naik, and J. Miller (2008), Tropical Pacific forcing of North American medieval megadroughts: Testing the concept with an atmosphere model forced by coral-reconstructed SSTs, *J. Clim.*, *21*, 6175–6190.

Seager, R., N. Naik, M. A. Cane, N. Harnik, M. Ting, and Y. Kushnir (2010), Adjustment of the atmospheric circulation to tropical Pacific SST anomalies: Variability of transient eddy propagation in the Pacific-North America sector, *Q. J. R. Meteorol. Soc.*, *136*, 277–296.

Smith, I., and E. Chandler (2010), Refining rainfall projections for the Murray-Darling Basin of south-east Australia—The effect of sampling model results based on performance, *Clim. Change*, *102*, 377–393.

Taylor, K. E., R. J. Stouffer, and G. A. Meehl (2012), An overview of CMIP5 and the experiment design, *Bull. Am. Meteorol. Soc.*, *93*, 485–498.

Trenberth, K. E., G. W. Branstator, D. Karoly, A. Kumar, N.-C. Lau, and C. Ropelewski (1998), Progress during TOGA in understanding and modeling global teleconnections associated with tropical Pacific sea surface temperatures, *J. Geophys. Res.*, *103*, 14,291–14,324.

Weare, B. C. (2012), El Niño teleconnections in CMIP5 models, *Clim. Dyn.*, doi:10.1007/s00382-012-1537-3.

Wittenberg, A. T. (2009), Are historical records sufficient to constrain ENSO simulations?, *Geophys. Res. Lett.*, *36*, L12702, doi:10.1029/2009GL038710.